



Comparison of antibacterial and antibiofilm activities of biologically synthesized silver nanoparticles against several bacterial strains of medical interest

Wallace R. Rolim^{1,2} · Claudio Lamilla^{3,4} · Joana C. Pieretti^{1,2} · Marcela Díaz^{3,4} · Gonzalo R. Tortella^{3,4} · M. Cristina Diez^{3,4} · Leticia Barrientos⁵ · Amedea B. Seabra^{1,2} · Olga Rubilar^{3,4}

¹ Center for Natural and Human Sciences (CCNH), Federal University of ABC (UFABC), Av. dos Estados 5001, Santo André, SP 09210-580, Brazil

² Nanomedicine Research Unit (NANOMED), Federal University of ABC (UFABC), Santo André, SP, Brazil

³ Department of Chemical Engineering, Universidad de La Frontera, Temuco, Chile

⁴ Biotechnological Research Center Applied to the Environment (CIBAMA-BIOREN), Universidad de La Frontera, Temuco, Chile

⁵ Laboratory of Applied Molecular Biology, Universidad de La Frontera, Avenida Alemania 0458, Temuco, Chile

Received: 18 April 2019/Revised: 4 June 2019/Accepted: 13 June 2019/Published online: 19 June 2019

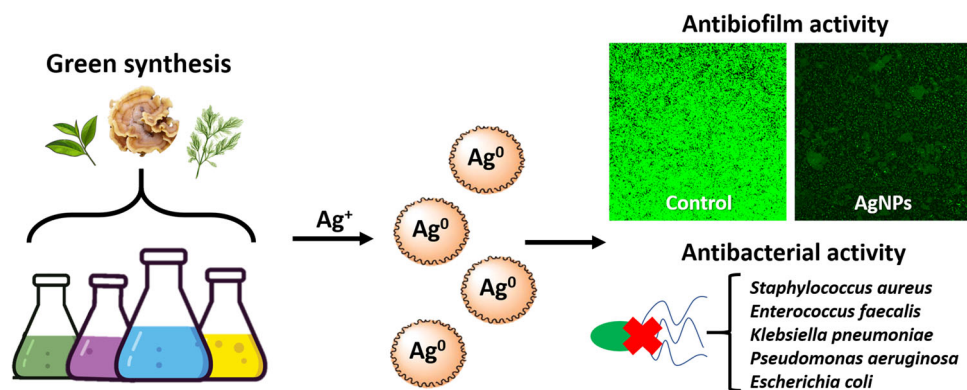
© The Joint Center on Global Change and Earth System Science of the University of Maryland and Beijing Normal University 2019

Abstract Biological routes have been extensively explored in the synthesis of metallic nanoparticles due to their simplicity and low cost. Among metallic nanoparticles, silver nanoparticles (AgNPs) are widely used in medical applications because of their potent antimicrobial activity. In this work, the ability of the mycelium-free fungus extract produced by Chilean white-root *Stereum hirsutum* and two plant extracts (green tea and dill) were used in the synthesis of AgNPs. The synthesized nanoparticles were extensively characterized by different techniques. The antibacterial activity of the nanoparticles was demonstrated against the Gram-positive strain *Staphylococcus aureus* ATCC 29213 and *Enterococcus faecalis* ATCC 3229 (standard CLSI); and the Gram-negative bacterial strains (standard CLSI) *Escherichia coli* ATCC

25922, *Klebsiella pneumoniae* ATCC 13803 and the multidrug-resistant *Pseudomonas aeruginosa* KPC 37. The values of minimal inhibitory concentration (MIC) and minimal bactericidal concentration (MBC) were obtained in the range of 1.56–25 $\mu\text{g mL}^{-1}$. AgNPs synthesized by dill extract showed lower values of MIC and MBC, compared to other nanoparticles. The potent antibiofilm ability of AgNPs was demonstrated, including against the multidrug-resistant *P. aeruginosa* KPC 37 strain. All synthesized nanoparticles demonstrated antibiofilm activity. AgNPs synthesized by fungus extract demonstrated superior antibiofilm activity, compared to AgNPs synthesized by green tea or dill, at low concentration (1.56 $\mu\text{g mL}^{-1}$). To our best knowledge, this is the first report to compare the antioxidant and antibacterial effects of AgNPs synthesized by different biological entities (green tea, dill and *S. hirsutum*) with great importance in the combat of resistant bacteria and biofilms.

✉ Amedea B. Seabra
amedea.seabra@ufabc.edu.br

Graphic abstract



Keywords Silver nanoparticles · Biogenic synthesis · *Stereum hirsutum* · Antibacterial · Antioxidant activity · Antibiofilm

1 Introduction

Silver nanoparticles (AgNPs) have been extensively employed in different commercial products such as healthcare products, in cleaning agents, textile coatings, food packing and storage and medical devices (Verma and Maheshwari 2019). AgNPs find important biomedical, environmental and commercial applications mainly due to their effective and broad-spectrum antimicrobial activity against bacteria, including resistant strains, pathogen fungi and viruses (Durán et al. 2016a, b). The successful uses of AgNPs in several commercial products, such as in antiseptic sprays, wound dressing bandages and dermatological creams, are derived from the ability of AgNPs to disrupt pathogenic membrane, hence impairing the microorganism's enzymatic activities (Flores-López et al. 2019).

In addition, the overuse of antibiotics has led to the emergence of antibiotic resistance that becomes a serious health issue worldwide (Furusawa et al. 2018). The major problem related to bacteria and drug resistance is the formation of biofilm, which is a complex bacteria community covered by polysaccharide matrix. This matrix protects the bacteria from antibiotic treatment and retains the nutrients required for the growth of the bacteria community (Parrino et al. 2019). Thus, bacteria biofilm contributes to antibiotic resistance, since 1000 times more antibiotics are required to kill bacteria, in comparison with planktonic cells (Smith 2005). Therefore, there is an increasing interest in the design of effective and low-cost strategies to combat resistant bacteria, including biofilms. Several works describe that due their small size and large surface area to volume ratio, AgNPs have potent antimicrobial activities

against Gram-negative, Gram-positive bacterial strains and also toward established biofilms (Durán et al. 2016a, b; Ali et al. 2018). Moreover, naturally occurring bacteria do not develop resistance to AgNPs (Mühling et al. 2009). Thus, AgNPs are considered one of the most effective engineered nanoparticles acting as broad-spectrum antimicrobial agent (Durán et al. 2016a).

AgNPs can be synthesized by chemical, physical and biological routes. Chemical reduction is one of the most traditional methods to synthesize AgNPs, and sodium borohydride and sodium citrate are usually employed as reducing agents (Baber et al. 2017). Usually, these methods also required the addition of capping/stabilizer agent to coat the surface of AgNPs avoiding nanoparticle agglomeration and aggregation (de Lima et al. 2012). Although chemical and physical routes are able to synthesize size controllable engineering nanoparticles with good reproducibility, these strategies might involve the presence of toxic chemicals, demand high-energy input, in some cases, controllable pressure and temperature, which might result in high costs, and the production of environmental contamination (Duran and Seabra 2018).

Biological routes to synthesize metallic nanoparticles, including AgNPs, involve the uses of plant extracts (green synthesis) or microorganisms, such as bacteria, fungi, and algae, as reducing and capping agents (de Lima et al. 2012; Ali et al. 2018; Duran and Seabra 2018). Biological methods have gained considerable importance in the last years due to their cost-effective and eco-friendly features. Usually, biological protocols to synthesize AgNPs are performed in aqueous medium (absence of organic solvents), at ambient temperature and pressure, in an easy protocol, free of toxicity (Alsammarrarie et al. 2018; Asghar et al. 2018). The biological source acts not only as a potent reducing agent (reducing Ag⁺ to Ag⁰, leading to the formation of AgNPs), but also as capping/stabilizing agent on the nanoparticle surface, avoiding nanoparticle agglomeration/aggregation, increasing the stability of the colloidal

suspension (de Lima et al. 2012; Cuevas et al. 2015; Duran and Seabra 2018).

Among the biological routes to synthesize AgNPs, the use of plant extract is considered efficient, versatile, low cost, simple, fast and easy to scale-up (Ebrahiminezhad et al. 2018). Nowadays, several different parts of plants (leaf, seed, fruit, bark, peel, flower, bran) have been used for the green synthesis of metallic nanoparticles (Niraimathi et al. 2013). In this sense, plant phytochemicals are strong reducing agents, leading to the formation of capped nanoparticles in a single- and one-pot reaction. In addition, plant extracts have their own medical value, due to the presence of phenolic compounds (polyphenols, flavonoids, tannic acid and terpenoids), vitamins, minerals and amino acids giving an additional functionality for the capped nanoparticle (Fierascu et al. 2010; Fahimirad et al. 2019).

Among the plant extracts that can be used for the green synthesis of AgNPs, green tea (*Camellia sinensis*) extract has been successfully employed for the biological synthesis of metallic nanoparticles (de Oliveira Silva and Seabra 2016; Rolim et al. 2019a, b). Green tea is rich in polyphenolic compounds, which is mainly comprised by epigallocatechin-3-gallate (EGCG), epigallocatechin, epicatechin-3-gallate and epicatechin (Ramírez-Aristizabal et al. 2015). The green tea phytochemicals have important medical benefits as effective antioxidant and anti-inflammatory agent, acting as protector agent of the immunological system, in the protection of intestine against food-borne pathogenic bacteria, and also in cosmetic and therapeutic applications (Singh et al. 2016).

The herb dill belongs to the family *Apiaceae*, genus *Anethum* and species *A. graveolens*. As green tea, dill is rich in polyphenols, minerals, vitamins (C, A, β -carotene, folic acid, niacin, riboflavin) and flavonoids (Ramadan et al. 2013; Kalangi et al. 2016). Dill has medical importance as an anti-hyperlipidemic agent, diuretic sedative and antispasmodic (Zayed et al. 2012; Kalangi et al. 2016). Recently, dill extract was used for the synthesis of AgNPs for antileishmanial activity (Kalangi et al. 2016). The authors reported that AgNPs enhanced the effect of miltefosine alone (traditional drug used to treat leishmaniasis), decreasing the IC_{50} of miltefosine about to half (Kalangi et al. 2016).

In addition to the mentioned above, the synthesis of AgNPs can also be obtained by mycelium-free extract of fungi. Microorganisms such as *Fusarium oxysporum* can be used in the biosynthesis of inorganic nanomaterials (Durán et al. 2005). The nonpathogenic white-root fungus *Stereum hirsutum* (*S. hirsutum*) has been used to biogenically synthesize copper and copper oxide nanoparticles (Cuevas et al. 2015). *S. hirsutum* is a native white-root fungus extensively found in Chilean forests. To our best

knowledge, this is the first report to describe the use of *S. hirsutum* for synthesis of AgNPs.

Therefore, the purpose of this study was to synthesize AgNPs by following biological routes by using plant extracts of green tea and dill and from mycelium-free extract produced by *S. hirsutum* and compare their antimicrobial and antibiofilm activities. The obtained nanoparticles were extensively characterized and showed potent antioxidant, antibacterial and antibiofilm activities. To our best knowledge, this is the first report to compare the antioxidant and antibacterial effects of AgNPs synthesized by different biological entities (green tea, dill and *S. hirsutum*) with great importance in the combat of resistant bacteria and biofilms.

2 Materials and methods

2.1 Materials

Silver nitrate ($AgNO_3$), phosphate buffer saline (PBS, pH 7.4), 2,2-diphenyl-1-picryl-hydrazyl-hydrate (DPPH), L-ascorbic acid, ferrozine, iron nitrate nonahydrate ($Fe(NO_3)_3 \cdot 9H_2O$, buffer acetate (pH 5.5) and Folin–Ciocalteu reagent were obtained from Sigma-Aldrich (St. Louis, MO, USA). Sodium hydroxide (NaOH), bromide potassium (KBr), hydrochloric acid (HCl), gallic acid, sodium bicarbonate and ethanol were obtained from Lab-synth (Diadema, SP, Brazil). Green tea powder (*Camellia sinensis*) was obtained from Sumioka Shokuhin Kabushikikaisha, Hiraguti, Japan. Commercial dill (*Anethum graveolens*) was purchased from local market at São Paulo, Brazil. *Stereum hirsutum*, a native fungus from southern Chilean forests, was obtained from the Chilean Collection of Culture Type (code CCCT16.03) of Universidad de La Frontera, Chile. Mueller–Hinton (broth and agar), glucose, potato peptone and yeast extract were obtained from Difco (Franklin Lakes, EUA). All experiments were carried out using analytical grade water from a Millipore Milli-Q Gradient filtration system (Millipore, 18.2 M Ω , USA).

2.2 Preparation of plant and mycelium-free extracts

To prepare the aqueous plant extracts of green tea (GT) and dill (D), the mass of 2 g of each plant powder was separately dissolved in 100 mL of water, under stirring and heating at 60 °C for 15 min. The extract suspensions were filtered using the Whatman No. 1 filter paper and cooled for later use. For the preparation of mycelium-free extract from fungus (F), five circular agar plugs (4 mm in diameter) taken from the margin of a growing colony of the *S. hirsutum* growing on malt extract agar were put into 500-mL Erlenmeyer flasks with 100 mL of growth medium

(pH 5.5) containing in g L^{-1} : glucose (15), potato peptone (5) and yeast extract (2.5) and incubating in dark for 14 days and 25 °C. The fungal biomass obtained at the end of the incubation period was filtered through Whatman No. 1 filter paper and washed thoroughly with deionized water. The fungal biomass was transferred into 100-mL Erlenmeyer flasks containing 50 mL of sterilized deionized water and incubated in an orbital shaker (150 rpm) for 24 h at 25 °C.

2.3 Characterization of the prepared extracts

Plant extracts (GT and D) were characterized as described below and used for the green synthesis of AgNPs.

2.3.1 Determination of total phenolic content

Folin–Ciocalteu procedure was used to determine the total phenolic compounds in plant extracts used to prepare AgNPs, as previously reported (San et al. 2013). Firstly, Folin–Ciocalteu reagent was diluted with deionized water (1:10). The extracts (green tea or dill) (20 mg mL^{-1}) or standard gallic acid solution ($10\text{--}150 \text{ }\mu\text{g mL}^{-1}$), as positive control, was mixed with 0.8 mL of sodium bicarbonate solution (7.5% w/v) in the presence of 0.5 mL of diluted Folin–Ciocalteu reagent. Absorbance values of final mixtures were measured with UV–Vis spectrophotometer (Agilent, model 8453, Palo Alto, CA, USA) at $\lambda = 765 \text{ nm}$. The total phenolic content in the different plants (GT, D) was calculated and expressed as milligrams of gallic acid equivalent (GAE) in 1 g of the dried powder. The results were obtained as mean \pm SD ($n = 3$).

2.3.2 Ferric reducing antioxidant power method (FRAP): Antioxidant activity

The antioxidant capacity of the plant extracts (green tea and dill) was evaluated by the FRAP assay, as previously described with some modifications (Vázquez et al. 2008). Briefly, 0.0202 g of $\text{Fe}(\text{NO}_3)_3 \cdot 9 \text{ H}_2\text{O}$ and 0.1231 g of ferrozine were dissolved in 1.0 mL of HCl (1.0 mol L^{-1}) and brought to 25.0 mL with deionized water. The final concentrations of $\text{Fe}(\text{NO}_3)_3 \cdot 9 \text{ H}_2\text{O}$ and ferrozine were $2.0 \times 10^{-3} \text{ mol L}^{-1}$ and $1.0 \times 10^{-2} \text{ mol L}^{-1}$, respectively. A volume of 0.25 mL of previously prepared extracts (GT or D) was added to 0.25 mL of water, 0.75 mL of ferrozine–Fe(III) solution and 1.0 mL of 0.2 mol L^{-1} acetate buffer at pH 5.5. The final mixtures were incubated for 30 min at 25 °C, and the intensities of the absorption bands at 562 nm were recorded by using the UV–Vis spectrophotometer. The relative activities of samples were calculated from the calibration curve of *L*-ascorbic acid ($0.025\text{--}0.2 \text{ mmol L}^{-1}$) (as positive control),

and the results are expressed as nmol ascorbic acid equivalent (AAE) mg^{-1} of extract (on a dry basis), as previously reported (Vázquez et al. 2008). The results were obtained as mean \pm SD ($n = 3$).

2.4 Synthesis of AgNPs by plant extracts

The volume of 75 mL of plant extracts (GT or D) was mixed with 0.1 mol L^{-1} of AgNO_3 , and the pH of the final suspensions was adjusted to 10.5 by dropping NaOH (1.0 mol L^{-1}). The obtained suspensions were stirred for 15 min and centrifuged at $9660 \times g$ for 10 min. The supernatant was discarded, and the obtained AgNPs were washed twice and freeze-dried. This process led to the formation of plant extract synthesized AgNPs by GT and D referred as AgNPs-GT and AgNPs-D, respectively.

2.5 Synthesis of AgNPs using *Stereum hirsutum*

The synthesis of AgNPs using the fungus strain *S. hirsutum* was prepared as described by Cuevas and coworkers (2015). A volume of 242.5 mL of *S. hirsutum* extract was transferred into 250-mL Erlenmeyer flasks. Then, 7.5 mL of a stock solution (100 mmol L^{-1}) of AgNO_3 was added to obtain a final concentration of 3.0 mmol L^{-1} and the pH was adjusted to 12.0 (NaOH 0.1 mol L^{-1}). The flasks were incubated for 24 h on an orbital shaker (150 rpm) at 25 °C in the dark. After, the synthesized nanoparticles were isolated by centrifugation, washed twice with water and lyophilized (Cuevas et al. 2015). The obtained AgNPs biogenically synthesized by the fungus *S. hirsutum* are referred as AgNPs-F.

2.6 Characterization of synthesized AgNPs

The plant extracts and fungus-synthesized AgNPs (AgNPs-GT, AgNPs-D and AgNPs-F) were characterized by different techniques, as described below.

2.6.1 UV–Visible spectroscopy analysis

All prepared AgNPs were characterized by UV–Visible spectroscopy analysis using a UV–Vis spectrophotometer, in the wavelength ranged from 200 to 800 nm with a resolution of 1 nm. AgNPs were dispersed in aqueous media with an ultrasound bath for 1 h, and the suspensions were transferred to quartz cuvettes for analysis.

2.6.2 X-ray diffraction (XRD)

AgNPs prepared by different extracts were characterized by XRD. A STADI-P (Stoe®, Darmstadt, Germany) diffractometer was used to record X-ray powder diffraction

operating at room temperature, 50 kV, 40 mA and using $\text{CuK}\alpha$ ($\lambda = 1.54060 \text{ \AA}$). The X-ray photons were collected by a Mythen 1 K (Dectris[®], Baden, Switzerland) detector. Data were recorded in the 2θ range from 15° to 90° , with step sizes of 0.015° and a counting time of 100 s at each 0.785° . In addition, the grain size of the synthesized AgNPs was calculated with the Debye–Scherrer equation (Eq. 1) (Naika et al. 2015; Rolim et al. 2019a).

$$D = (k\lambda)/(\beta \cos \theta) \quad (1)$$

where D is the diameter of crystallite size, λ is the wavelength for $\text{CuK}\alpha$, β is the full width at half maximum (FWHM) of the peak, θ is the Bragg diffraction angle, and K is a constant. (0.94 is used to correspond spherical crystallites with cubic symmetry.)

2.6.3 Fourier-transform infrared spectroscopy (FTIR)

The synthesized AgNPs and the pure biological extracts (GT, D and F) were triturated with pure potassium bromide (KBr) powder. These mixtures were ground into fine powders, pressed in a mechanical press to generate translucent pellets and analyzed using an Agilent Cary 630 spectrometer (Palo Alto, CA, USA). A pure pellet of KBr was used for background. The FTIR spectra were recorded from 700 to 4000 cm^{-1} at a resolution of 4 cm^{-1} .

2.6.4 Atomic force microscopy (AFM)

The size of AgNPs obtained by different extracts was determined by atomic force microscopy, using an AFM/STM Series 5500 dynamics (Agilent Technologies, Palo Alto, CA, USA). The non-contact mode was employed using silicon tips of 4 nm thickness, 125 μm length, 30 μm width, resonance frequency of 320 kHz and force constant of 42 N m^{-1} . Nanoparticles were dispersed in an ultrasound bath (0.5 mg mL^{-1}), diluted (1:999), and 10 μL was drop-casted onto a silicon wafer and dried in room temperature. Images obtained were analyzed using WSxM 5.0 software, and average size and standard error were evaluated using OriginPro 8.0 software.

2.6.5 X-ray photoelectron spectroscopy (XPS)

XPS (Thermo K-alpha spectrometer, MA, USA) was carried out to measure the elemental composition of the AgNPs prepared via different extracts. The measurements were taken in powdered samples where the instrument utilized a 72 W monochromated Al K-alpha⁺ source ($E = 1486.6 \text{ eV}$) with energy adjusted to 3000 eV, medium current, a spot size of 400 μm and depth of 10 nm was set. The analyses were performed in two different points of the

samples, and the data were analyzed using CasaXPS software, representing the average of all measurements.

2.6.6 Dynamic light scattering (DLS)

A Zetasizer Nano ZS (Malvern Instruments Co., UK) was used to analyze the average hydrodynamic size (evaluated by % of number), and polydispersity index (PDI), and zeta potential of the obtained nanoparticles in aqueous media at 25°C . Measurements were taken using disposable folded capillary zeta cell (10 mm path length) and using a fixed angle of 173° .

2.7 Antioxidant activity of AgNPs prepared by plant and fungus extracts

The antioxidant activity of AgNPs-GT, AgNPs-D and AgNPs-F was measured using DPPH (2,2-diphenyl-1-picryl-hydrazyl-hydrate) radical photometric assay, indicating antioxidant activity through its discoloration (Guo et al. 2013; Nakurte et al. 2017). A volume of 500 μL of 0.1 mmol L^{-1} DPPH ethanolic solution was added to 500 μL of aqueous suspension of AgNPs-GT, AgNPs-D or AgNPs-F, with different final concentrations of 2.0, 20, 40 or 80 $\mu\text{g mL}^{-1}$ diluted in PBS. A control group was prepared by using PBS and DPPH ethanolic solution. The final mixtures were kept at room temperature, protected from light for 30 min and placed into quartz cuvettes. The absorbance intensities at 517 nm for all samples were recorded by using an UV–Vis spectrophotometer. The obtained absorbance values were converted to the percentage of antioxidant activity (AA) through the following equation (Sudha et al. 2017):

$$\text{AA}\% = [(Abs_{\text{control}} - Abs_{\text{sample}}) / Abs_{\text{control}}] \times 100 \quad (2)$$

where Abs_{sample} is the absorbance of the sample in ethanolic DPPH and Abs_{control} is the absorbance of ethanolic DPPH, in the absence of the nanoparticles. The results were plotted as sample concentration on the x-axis and the respective percentage of inhibition on y-axis. The assay was performed in triplicate.

2.8 Antibacterial activity

The minimal inhibitory concentration (MIC) and minimal bactericidal concentration (MBC) for AgNPs-GT, AgNPs-D and AgNPs-F were carried out by microdilution assay as described by the Clinical and Laboratory Standards Institute (CLSI 2012). The bacterial strains evaluated were the Gram-positive strain *S. aureus* ATCC 29213 and *Enterococcus faecalis* ATCC 3229 (standard CLSI); and the Gram-negative bacterial strains (standard CLSI) *Escherichia coli* ATCC 25922, *Klebsiella pneumoniae* ATCC

13803 and the multidrug-resistant (MDR) *Pseudomonas aeruginosa* KPC 37. Initially, the bacteria were grown in Mueller–Hinton solid medium at 37 °C to obtain the isolated colonies. Subsequently, the colonies were solubilized in a Mueller–Hinton and adjusted to the 0.5 index of the MacFarland scale (1.5×10^8 colony-forming units (CFU) mL^{-1}). This solution was diluted 10x in Mueller–Hinton broth and distributed in a 96-well plate. Each well was treated with different concentrations of AgNPs (1.56 to 100.0 $\mu\text{g mL}^{-1}$). The plates were incubated for 18 h, and the bacterial growth was measured after this period. The MBC tests were performed after the MIC tests. After 24 h of incubation, drops of bacterial broth from the cavity with no visual growth were added to a Petri dish with the Mueller–Hinton solid medium, and bacterial growth was observed after 24 h. After, the tolerance level of *S. aureus*, *E. faecalis*, *K. pneumoniae*, *P. aeruginosa* and *E. coli* against the biosynthesized AgNPs was determined according to the method of Neethu and coauthors (2018).

2.9 In vitro biofilm formation assay: Antibiofilm activity of the nanoparticles

The antibiofilm activities of AgNPs-GT, AgNPs-D and AgNPs-F were evaluated as described by Stepanović and coworkers (2000). After the MIC and MBC tests, the obtained 96-well plates with *S. aureus*, *E. Faecalis*, *E. coli*, *K. pneumoniae* and *P. aeruginosa* KPC 37 were washed three times with 200 μL of distilled water. Then, 200 μL of methanol was added to for 15 min and left to dry at room temperature. After, the adhered cells were stained with 200 μL of 1% crystal violet for 20 min and washed with distilled water three times. The biofilm-associated/crystal violet was solubilized with 33% v/v glacial acetic acid per well, and the optical density (OD) was measured at 570 nm using a microplate reader (Stepanović et al. 2000).

2.10 Imaging of MDR *P. aeruginosa* KPC 37 biofilm using scanning confocal laser microscopy

An overnight culture of MDR *P. aeruginosa* KPC 37 was diluted in Mueller–Hinton medium, and after that the cells were grown on glass slides during 24 h at 37 °C forming the biofilms. The culture supernatant was removed, and a fresh Mueller–Hinton medium was added with AgNPs-GT with concentrations of 50 and 100 $\mu\text{g mL}^{-1}$. The cells were further grown during 24 h. The biofilm viability was assessed with Live/Dead BacLight Bacterial Viability and Counting Kit (Invitrogen, Molecular Probes) provided for scanning confocal laser microscopy (Olympus, FV1000, Japan) with an excitation wavelength at 488 nm. The images were processed using Image Processing software (FV10-ASW v.0.2c).

3 Results and discussion

3.1 Total phenols contents and antioxidant activity of plant extracts

The phenolic compounds present in plant extracts have antioxidant activity and the capacity of reduced ions, in this case, to reduce Ag^+ ion into Ag^0 (Ignat et al. 2011; Machado et al. 2013). The phenolic content and the antioxidant activity of the plant extracts used to synthesize the AgNPs were measured by the Folin–Ciocalteu method (Fig. 1a) and by the FRAP method (Fig. 1b), respectively. The results demonstrated a higher phenolic content in green tea extract (164.9 ± 6.9 mg GAE g^{-1} of extract) compared with dill extract (54.9 ± 5.0 mg GAE g^{-1} of extract) (Fig. 1a). Commercial green tea is known to have ca. 11–130 mg GAE g^{-1} (Pal et al. 2012; Ramírez-Arízabal et al. 2015).

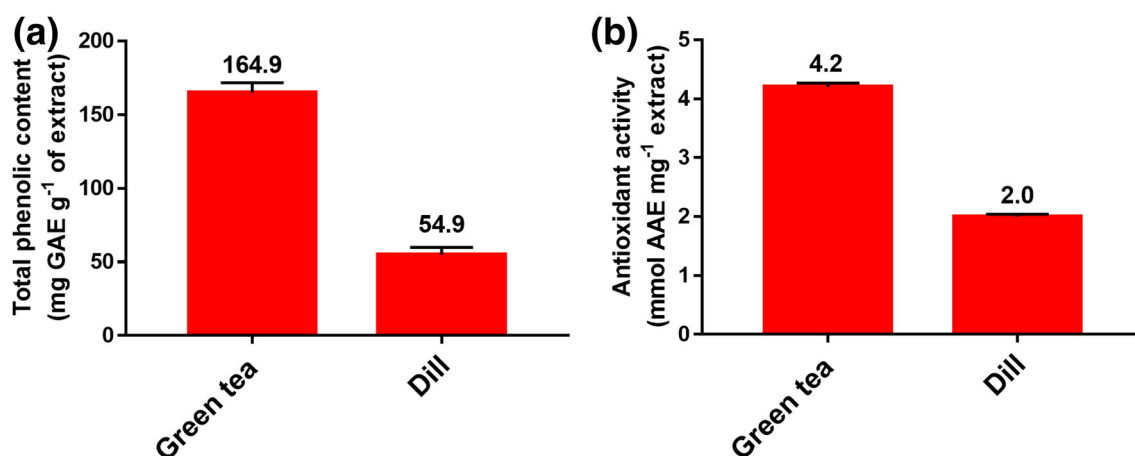


Fig. 1 Total phenolic content (a) and ferric reducing antioxidant power (b) of green tea and dill extracts

In the case of antioxidant activity, the green tea extract demonstrated a superior iron-reducing capacity, with a reduction of 4.2 ± 0.1 mmol AAE mg^{-1} of extract, compared with dill extract (2.0 ± 0.1 mmol AAE mg^{-1} of extract) (Fig. 1b). Thus, green tea extract showed higher total phenolic content and antioxidant ability, compared with dill extract. As expected, antioxidant activity of the compound depends on the amount of phenolic compounds in the plants. It should be noted that a different antioxidant capability of polyphenols depends on their chemical structure, regarding the number and position of phenolic hydroxyl groups (Ramírez-Aristizabal et al. 2015). Similar results have been described by several papers in the measurements of total phenolic content and/or antioxidant activity of different plant extracts, employed for the biosynthesis of metallic nanoparticles (Vázquez et al. 2008; Pal et al. 2012; Kumar et al. 2016). Green tea and dill demonstrated antioxidant capability due to the presence of polyphenol groups, and thus ability to synthesize AgNPs, as described below.

3.2 Green synthesis of AgNPs

In this work, the plant extracts (green tea and dill) and the mycelium-free extract of the fungus *S. hirsutum* were screened for their bioreduction in the synthesis of AgNPs. Indeed, plant extracts are rich in polyphenols that act as reducing and capping agents of the nanoparticles (Alsammarraie et al. 2018; Asghar et al. 2018; Duran and Seabra 2018). Moreover, due to the intrinsic features of the plant extract, its presence on nanoparticle surface might gain additional biological importance to the nanomaterial (Fierascu et al. 2010; Fahimirad et al. 2019). In addition, a mycelium-free extract of *S. hirsutum* was employed for the

synthesis of AgNPs. The main biological entity responsible for the bioreduction in Ag^+ is reported to be electron shuttle in conjugation with nitrate reductase (Durán et al. 2005).

3.3 Characterization of green synthesized AgNPs

3.3.1 UV-Vis spectroscopy analysis

Firstly, the formation of AgNPs was confirmed by color changes in the starting material (Ag^+) from colorless to brownish black, characteristic of colloidal AgNPs (Saeb et al. 2014; Asghar et al. 2018). In addition, the formation of AgNPs was confirmed by the detection of the surface plasmonic resonance (SPR) band that typically occurs between 390 and 510 nm (Oliver et al. 2018). This band is associated with the oscillation of the electrons on the surface of the nanoparticles, upon excitation in a determined wavelength (Dubey et al. 2010). Figure 2 shows the SPR bands are centered at 404, 416 and 404 nm for AgNPs-GT, AgNPs-D and AgNPs-F, respectively. It is possible to observe a similar absorption profile for all synthesized AgNPs with no significant shiftiness of wavelengths. Similar profile for SPR bands indicates a similar shape for all green synthesized AgNPs. The higher intensity of AgNPs-F observed in Fig. 2 is due to the higher concentration of AgNPs in the suspension, compared with AgNPs synthesized by plant extracts. Our results suggest the formation of small and uniformly spherical nanoparticles (Rolim et al. 2019a).

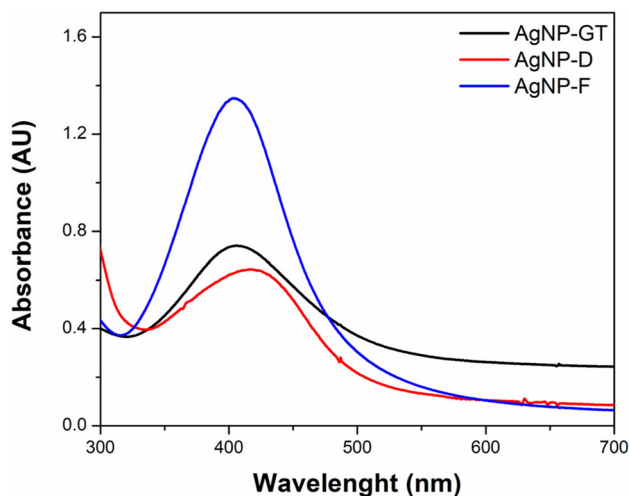


Fig. 2 UV-Vis absorption spectra of AgNPs-GT (black line), AgNPs-D (red line) and AgNPs-F (blue line)

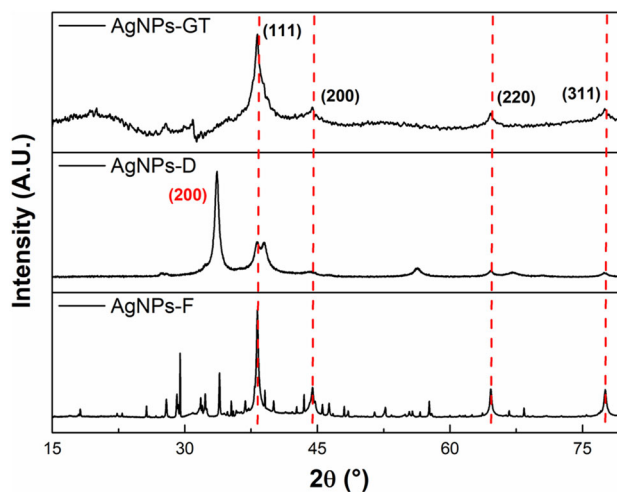


Fig. 3 XRD patterns of the synthesized AgNPs using a Cu source (1.5418 \AA). Miller indexes for all Bragg reflections are indicated in the figure

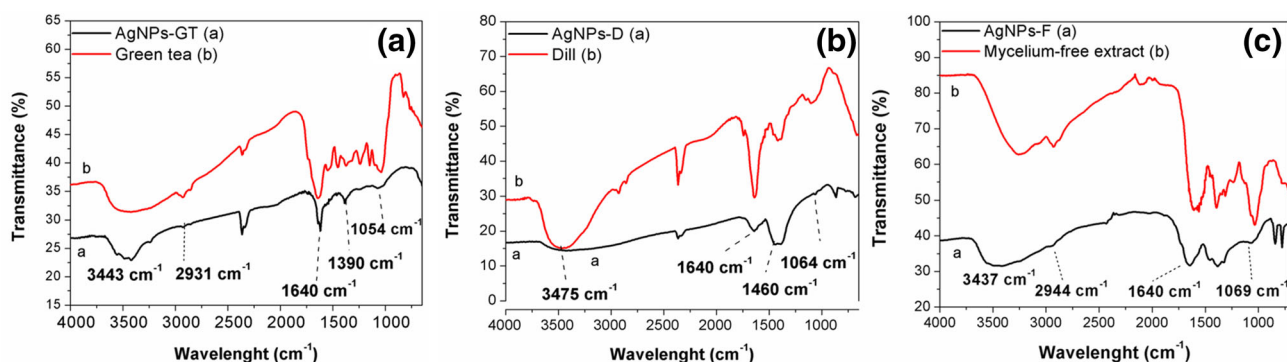


Fig. 4 FTIR spectra of synthesized AgNPs-GT **a**, AgNPs-D **b** and AgNPs-F **c** and their respective powder extracts

3.3.2 X-ray diffraction (XRD)

The crystalline nature of AgNPs was confirmed by XRD (Fig. 3). The XRD analyses for AgNPs-GT, AgNPs-D and AgNPs-F revealed similar 2θ peaks values at 38.1° , 44.4° , 64.6° and 77.4° , which is associated with the planes [111], [200], [220] and [311] facets of AgNPs (Vázquez et al. 2008; Rolim et al. 2019a, b). In addition, the XRD pattern of AgNPs-D shows an additional peak at 32.7° that might be attributed to the presence of silver chloride (AgCl) (Durán et al. 2016b). This result suggests surface oxidation on these nanoparticles. Similar results were obtained by Oliver and coauthors (2018). Moreover, the crystallite-sized nanoparticles calculated by the Debye–Scherrer equation for AgNPs-GT, AgNPs-D and AgNPs-F were found to be 4.52, 11.11 and 18.97 nm, respectively. Interesting, it is possible to observe broader peaks for AgNPs-D and AgNPs-GT and this behavior can be associated with small crystallite sizes (Oliver et al. 2018). In contrast, it is possible to observe a narrow peak of the plane [111] for AgNPs-F, which corresponds to a higher crystallite size. The obtained results indicate the successful formation of AgNPs with a face-centered cubic structure with crystallite at the nanoscale (Durán et al. 2016b).

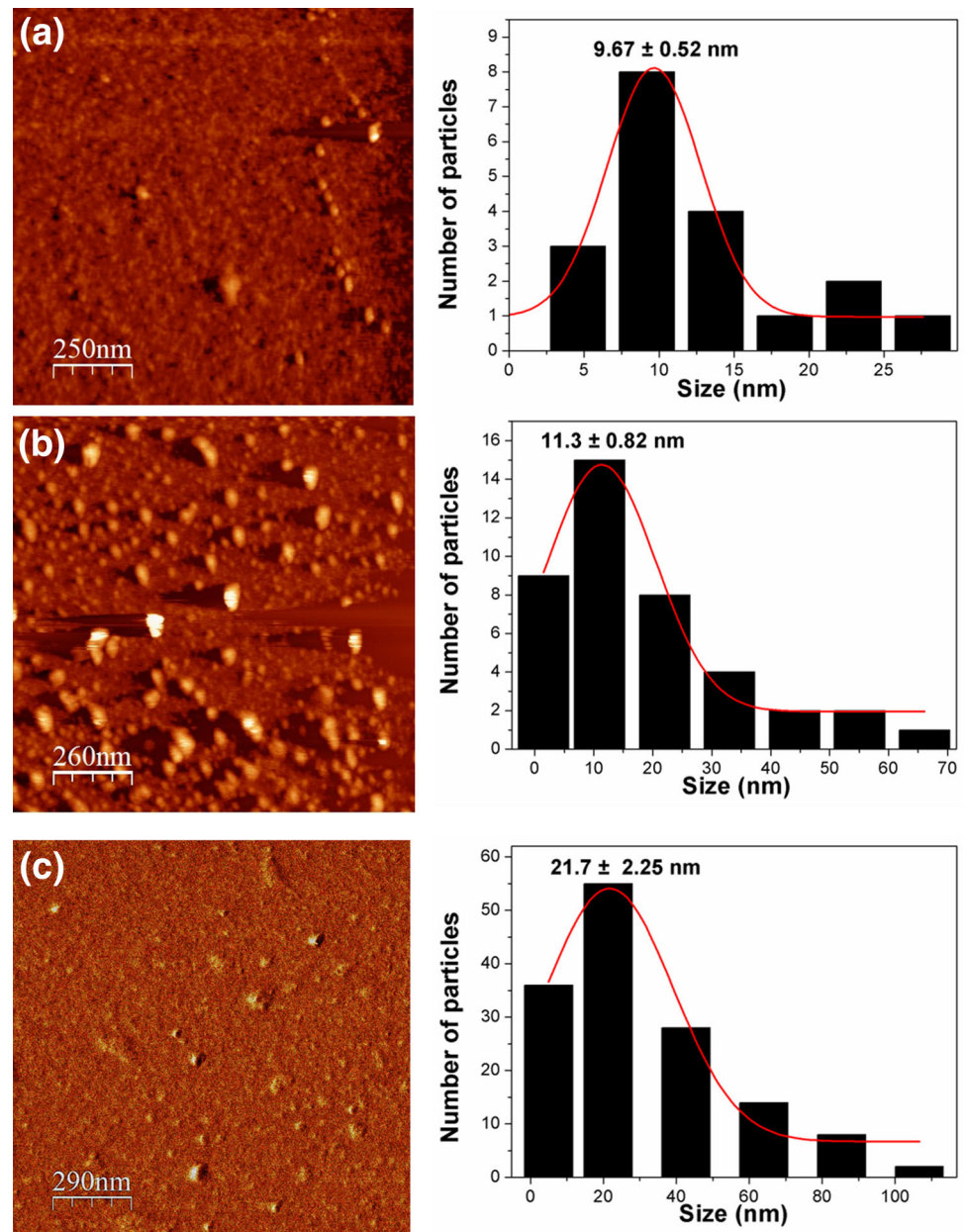
3.3.3 Fourier-transform infrared spectroscopy (FTIR)

FTIR analyses were performed to confirm the presence of phytochemicals and fungus extract on the surface of AgNPs, which act as reducing and capping agents. Biomolecules derived from plant and fungal extracts play major roles in the reduction of Ag^+ and the stabilization of the obtained AgNPs (Singh et al. 2018). Figure 4 shows the FTIR analyses for all plant and fungus-synthesized AgNPs, and their corresponding plant extracts. As can be observed in Fig. 4a, b, plant-mediated AgNPs have similar profile compared with their corresponding plant extract, indicating the presence of phytochemicals on the surface of plant-mediated AgNPs.

Figure 4a, b shows the spectra of pure green tea and the AgNPs-GT, and for pure dill and AgNPs-D, respectively. It is possible to observe five major peaks at 3443 cm^{-1} , 2931 cm^{-1} , 1640 cm^{-1} , 1390 cm^{-1} and 1054 cm^{-1} . The peaks at 3443 cm^{-1} and 2931 cm^{-1} are attributed to hydroxyl groups (O–H stretching) assigned to –OH group of polyols such as catechins, and C–H/ CH_2 vibration of aliphatic hydrocarbons, respectively (Rolim et al. 2019a, b; Kalangi et al. 2016; de Oliveira Silva and Seabra 2016). In addition, the peaks at 1640 cm^{-1} and 1390 cm^{-1} are attributed to C=O groups from carboxylic acids and C–N stretching, derived from caffeine present in green tea (de Oliveira Silva and Seabra 2016; Rolim et al. 2019a, b). The peak at 1054 cm^{-1} could be attributed to C–O–C stretching vibration (de Oliveira Silva and Seabra 2016). Comparing the spectra of AgNPs with the corresponding powder extract, it is possible to observe a decrease in the hydroxyl band. This behavior is related to the possibility that the hydroxyl groups of dill extract might undergo oxidation reaction of the phenols and subsequently, reduction of the Ag^+ ions into Ag^0 (Seabra et al. 2017).

Furthermore, the FTIR spectrum of AgNPs-F (Fig. 4c) revealed bands in the regions of 3437 cm^{-1} and 2944 cm^{-1} , which might be attributed to movements of stretching vibrations in primary and secondary amines (Cuevas et al. 2015). The peak at 1640 cm^{-1} is associated with bending vibrations, and the bands near 1069 cm^{-1} are attributed to aliphatic amines (Cuevas et al. 2015). These results are in accordance with the previous reports that demonstrated the presence of biomolecules, such as proteins and polyphenols in the biological extracts that act as reducing and capping agents on the surface of the synthesized nanoparticles (Zayed et al. 2012; Oves et al. 2013; Rajasekharreddy and Rani 2014; Sarsar et al. 2015). These biological capping agents could possibly form a layer covering the metal nanoparticles preventing nanoparticle agglomeration and thereby stabilizing the medium.

Fig. 5 Atomic force microscopy (AFM) images (left) and size distribution at solid state (right) of synthesized AgNPs-GT (a), AgNPs-D (b) and AgNPs-F (c)



3.3.4 Atomic force microscopy (AFM)

AFM was used to characterize the morphology and size distribution of green synthesized AgNPs, at solid state. Topography, phase contrast and amplitude micrographs were simultaneously recorded, and the average size distribution of AgNPs was calculated. Figure 5 shows the representative micrographs and the estimated size distribution of AgNPs-GT (a), AgNPs-D (b) and AgNPs-F (c). The micrographs indicated the formation of spherical and well-dispersed AgNPs. The values of average size distribution were found to be 9.67, 11.3 and 21.7 nm for AgNPs-GT, AgNPs-D and AgNPs-F, respectively (Fig. 5). The results indicated a larger size distribution for AgNPs

synthesized via fungus extract, compared with AgNPs synthesized by plant extracts. These results are in accordance with the previous reports based on fungi-mediated biosynthesis of AgNPs (Basavaraja et al. 2008; Krishna et al. 2015; Garg and Garg 2018).

Comparing the average size distribution of AgNPs synthesized by plant extracts, it is possible to notice that the average size was gradually increased from green tea to fungus extracts employed in the synthesis. According to the crystallization theory, the final particle size depends on several parameters including nucleation, growth rates and the nature of the reducing agent. Generally, slow nucleation process leads to a small number of nuclei that may grow and lead to larger nanoparticles, while fast nucleation

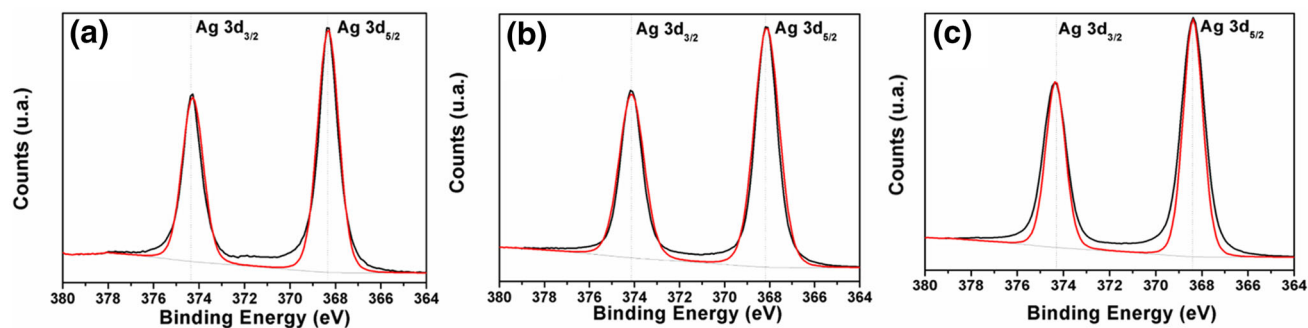


Fig. 6 High-resolution Ag 3d spectra of synthesized AgNPs-GT (a), AgNPs-D (b) and AgNPs-F (c) obtained by XPS measurements

tends to yield a large number of nuclei, which may result in smaller nanoparticles (Mehta et al. 2010). In this sense, the average size distribution prepared AgNPs might be intrinsically related to the nature of the biological extract chosen for the synthesis. In addition, Fig. 1 shows a higher total phenolic content (Fig. 1a) and a superior antioxidant activity (Fig. 1b) for AgNPs-GT, compared with nanoparticles synthesized by dill extract. These results suggest that nucleation process might be faster for green synthesis using green tea extract, which possesses a higher capability of reducing Ag^+ ions to Ag^0 leading to large number of nuclei and smaller nanoparticles. Similarly, Mehta and coauthors reported different size distributions of AgNPs when prepared by different plant extracts (Mehta et al. 2010).

3.3.5 X-ray photoelectron spectroscopy (XPS)

The XPS characterization was carried out to reveal the actual oxidation state of silver at the prepared nanoparticles. The survey spectra (data not shown) of AgNPs-GT, AgNPs-D and AgNPs-F indicated the presence of carbon (C), silver (Ag), oxygen (O) and nitrogen (N) for all samples. Figure 6 shows the spectra in Ag 3d region for AgNPs-GT (a), AgNPs-D (b) and AgNPs-F (c). It was possible to observe two characteristic peaks at 374.3 eV

and 368.2 eV, which can be assigned, respectively, to Ag $3d_{3/2}$ and Ag $3d_{5/2}$ core-level binding energies, well corresponded to metallic silver, being consistent with XRD results (Fig. 3), in agreement with the previous reports in the literature (Han et al. 2011; Rajasekharreddy and Rani 2014; Ansari et al. 2018). Zhang and coworkers also reported a 6.1 eV splitting of 3d doublet to characterize metallic Ag, and this splitting was observed for all nanoparticles in Fig. 6, suggesting that metallic silver (AgNPs) were successfully synthesized through all different plant and fungus extracts (Zhang et al. 2011).

3.3.6 Dynamic light scattering (DLS)

The DLS measurements revealed that all synthesized AgNPs are at nanoscale, with hydrodynamic average size less than 60 nm, and with a monomodal size distribution (Fig. 7a–c). As can be seen in Fig. 7, the values of average hydrodynamic size distribution for the nanoparticles are higher compared with the nanoparticle size obtained from AFM analysis (at solid state) (Fig. 5). As expected, higher values of nanoparticle size are obtained from DLS measurements related to the size values obtained at solid state (Rolim et al. 2019a). The presence of extra hydrate layers, along with ions or molecules attached to the nanoparticle

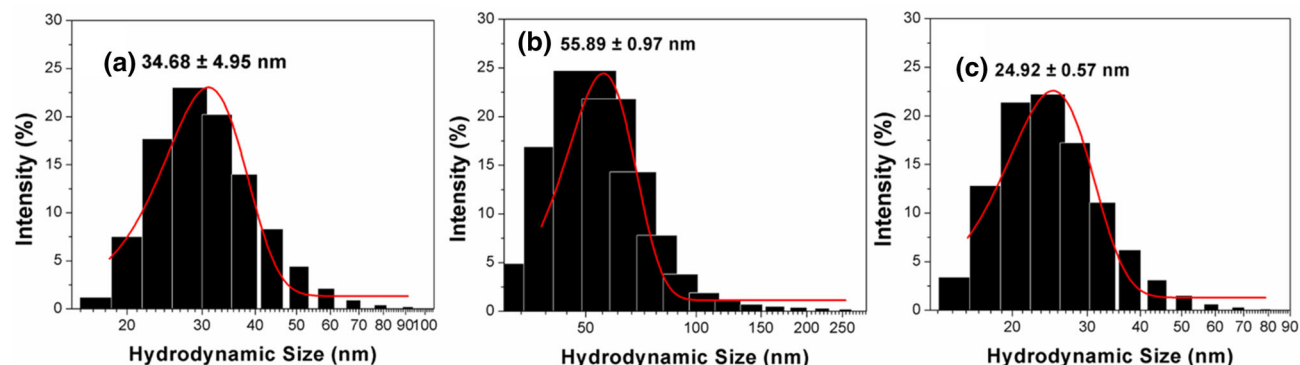
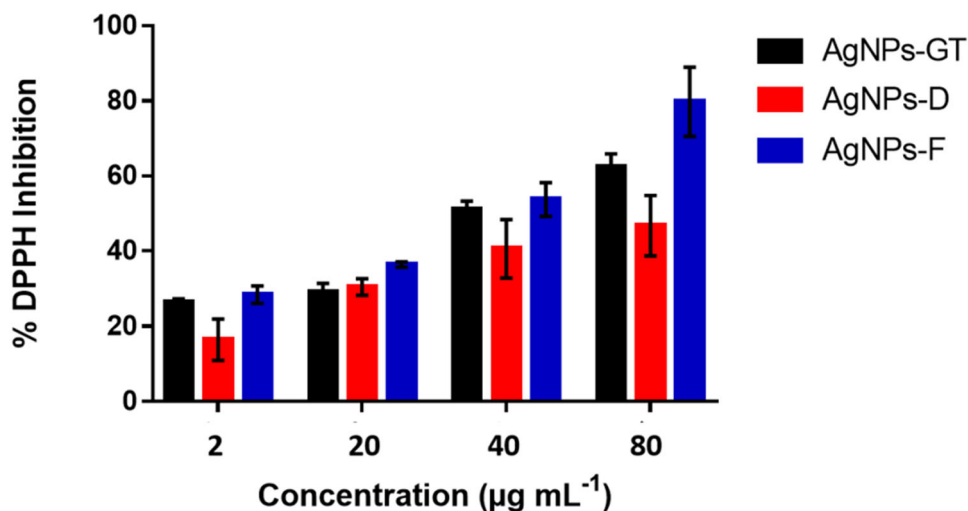


Fig. 7 Hydrodynamic size distribution of AgNPs-GT (a), AgNPs-D (b) and AgNPs-F (c)

Fig. 8 DPPH radical scavenging activity of AgNPs-GT (black bar), AgNPs-D (red bar) and AgNPs-F (blue bar)



surface in an aqueous environment, was responsible for the higher hydrodynamic sizes (Rolim et al. 2019a).

The PDI values for AgNPs-GT, AgNPs-D and AgNPs-F were found to be 0.28 ± 0.01 , 0.37 ± 0.01 and 0.52 ± 0.04 , respectively. These values indicate a moderate polydispersity. Zeta potential values of -35.5 ± 1.18 mV, -23.5 ± 0.40 mV and -35.93 ± 3.51 mV were obtained for AgNPs-GT, AgNPs-D and AgNPs-F, respectively. The negative zeta potential value is expected due to the presence of polyphenols and proteins attached on nanoparticles surface (Fernández et al. 2016; de Oliveira Silva and Seabra 2016). In addition, the magnitude of the obtained zeta potential values indicates high stability of synthesized AgNPs in aqueous suspension. Our results obtained by DLS are in accordance with similar green synthesized AgNPs (Rajasekharreddy and Rani 2014; de Oliveira Silva and Seabra 2016; Seabra et al. 2017; Singh et al. 2018).

3.4 Antioxidant activity of green synthesized AgNPs

The use of DPPH protocol provides a rapid and easy method to evaluate the antioxidant activity of the synthesized AgNPs. Plant phytochemicals and fungus enzymes act as reducing and capping agents of the nanoparticles.

This capping layer on the nanoparticle surface is responsible for antioxidant activity of AgNPs (Mittal et al. 2012). Figure 8 shows the percentage of DPPH radical inhibition upon incubation with different concentrations of AgNPs-GT, AgNPs-D and AgNPs-F. The results demonstrate a concentration-dependent free radical scavenging action (antioxidant activity) for all tested nanoparticles. Overall, AgNPs-F and AgNPs-GT showed superior antioxidant activity. This behavior can be associated with the high content of reducing enzyme in fungus extract (Durán et al. 2005; Cuevas et al. 2015) and high phenolic content in green tea extract (Masek et al. 2017). At nanoparticle concentration of $80 \mu\text{g mL}^{-1}$, the percentages of free radical scavenging activity of AgNPs-GT, AgNPs-D and AgNPs-F were found to be 62.41, 46.74 and 79.73%, respectively.

These results demonstrated that all synthesized AgNPs have antioxidant activity, highlighting the potent antioxidant activity of AgNPs-F and AgNPs-GT. Our results are in agreement with the previous published work based on AgNPs synthesized by green routes (Niraimathi et al. 2013; Mittal et al. 2014; Sudha et al. 2017). These results indicate that all AgNPs prepared in this work might be used as potent antioxidant agents.

Table 1 MIC values ($\mu\text{g mL}^{-1}$) for synthesized AgNPs evaluated against different bacterial strains

	MIC ($\mu\text{g mL}^{-1}$)		
	AgNPs-GT	AgNPs-D	AgNPs-F
<i>Staphylococcus aureus</i> (ATCC 25923)	1.56	1.56	3.125
<i>Enterococcus faecalis</i> (ATCC3229)	3.125	1.56	12.5
<i>Klebsiella pneumoniae</i> (ATCC 13803)	25	1.56	25
<i>Pseudomonas aeruginosa</i> (KP 37)	1.56	1.56	1.56
<i>Escherichia coli</i> (ATCC 25922)	1.56	1.56	3.125

Table 2 MBC values ($\mu\text{g mL}^{-1}$) for synthesized AgNPs evaluated against different bacterial strains

	MBC ($\mu\text{g mL}^{-1}$)		
	AgNPs-GT	AgNPs-D	AgNPs-F
<i>Staphylococcus aureus</i> (ATCC 25923)	3.125	1.56	6.25
<i>Enterococcus faecalis</i> (ATCC3229)	6.25	1.56	12.5
<i>Klebsiella pneumoniae</i> (ATCC 13803)	25	1.56	25
<i>Pseudomonas aeruginosa</i> (KP 37)	1.56	1.56	3.125
<i>Escherichia coli</i> (ATCC 25922)	3.125	1.56	6.25

3.5 Antibacterial activity

The antibacterial activities of AgNPs-GT, AgNPs-D and AgNPs-F were evaluated against Gram-positive *S. aureus* (ATCC 25923) and *Enterococcus faecalis* (ATCC 3229), and against Gram-negative *Klebsiella pneumoniae* (ATCC 13803), *Escherichia coli* (ATCC 25922) and the multidrug-resistant *P. aeruginosa* (KPC 37) bacterial strains at different nanoparticle concentrations. MIC and MBC values are shown in Tables 1 and 2, respectively. The results presented on Tables 1 and 2 show a potent antibacterial activity of all synthesized AgNPs against different bacterial strains. Interestingly, by comparing the MIC and MBC values, it is possible to observe that the *P. aeruginosa* was more sensitive for all synthesized AgNPs. In contrast, the bacterial strain *Klebsiella pneumoniae* demonstrated to be less susceptible to AgNPs-GT and AgNPs-F with MIC and MBC values of $25 \mu\text{g mL}^{-1}$. Even though, all green synthesized AgNPs demonstrated relatively low MIC and MBC values, suggesting their potent antibacterial activity. Recently, Rolim and coworkers reported MIC and MBC values in the range of $7\text{--}500 \mu\text{g mL}^{-1}$ and $15\text{--}500 \mu\text{g mL}^{-1}$ for AgNPs-GT against different Gram-positive and Gram-negative bacterial strains (Rolim et al. 2019a). MIC values in the range of $20\text{--}25 \mu\text{g mL}^{-1}$ were reported for AgNPs synthesized by using bark extract of the medicinal plant *Holarrhena pubescens* Wall ex G. Don (HP) against clinical isolates of *P. aeruginosa* (Ali et al. 2018). A MIC value of $6.25 \mu\text{g mL}^{-1}$ was reported for AgNPs synthesized by using spice blend extract against *Streptococcus faecalis*, *Bacillus cereus*, *Escherichia coli* and *Shigella flexneri* (Ali et al. 2018). Overall, our results are in accordance with the previous reports (de Lima et al. 2012).

Furthermore, the tolerance level (ratio between MBC and MIC values) of all bacterial strains used in this work was estimated. The tolerance level equal or greater than 16 indicate a bacteriostatic effect, while tolerance level equal or less than 4, suggest a bactericidal effect (Neethu et al. 2018). According to Tables 1 and 2, all synthesized AgNPs

have tolerance level values equal or less than 2, for all tested bacterial strains. Therefore, our results demonstrate that all synthesized AgNPs are bactericidal in nature with a potent antibacterial activity against both Gram-positive and Gram-negative bacteria.

The mechanism of antibacterial activity of AgNPs is reported to involve the following steps: (i) attachment of the nanoparticles to bacterial cell membrane through interactions with sulfur-containing proteins, (ii) disturbance of membrane permeability leaking the intracellular content and impairment of cell respiration, (iii) DNA damage, (iv) generation of reactive oxygen species, (v) regulation of phosphotyrosine profiles of proteins, (vi) cell cycle progression, (vii) synthesis of capsular polysaccharides, (viii) impairment of protein synthesis and functions and (ix) cell death (Durán et al. 2016a; Alsammarrarie et al. 2018). In addition, the biological effects of nanoparticles are dependent on nanoparticle size, nanoparticle morphology, degree of agglomeration, surface chemistry and surface charge, among others (de Lima et al. 2012). In this sense, small size nanoparticles might increase the nanoparticle interaction and penetration in membrane cell wall. As the surface nature of nanoparticles is important for particle biological activity, the presence of phytochemicals from plant extracts or proteins from fungus extract might enhance the antibacterial activity of the nanoparticle. The phytochemicals derived from green tea and dill have antimicrobial activities. For instance, the phytochemical catechin gallate might undergo intercalation into phospholipid membrane bilayers of bacteria membrane, disturbing functions of key processes related to the bacterial cytoplasmatic membrane (Durán et al. 2016a). Pure plant extracts are known to have antimicrobial effects, which might be enhanced upon coupled with AgNPs.

3.6 In vitro biofilm formation assay

AgNPs are well known to have antibiofilm effects (Gurunathan et al. 2014). A biofilm allows bacterial persistence

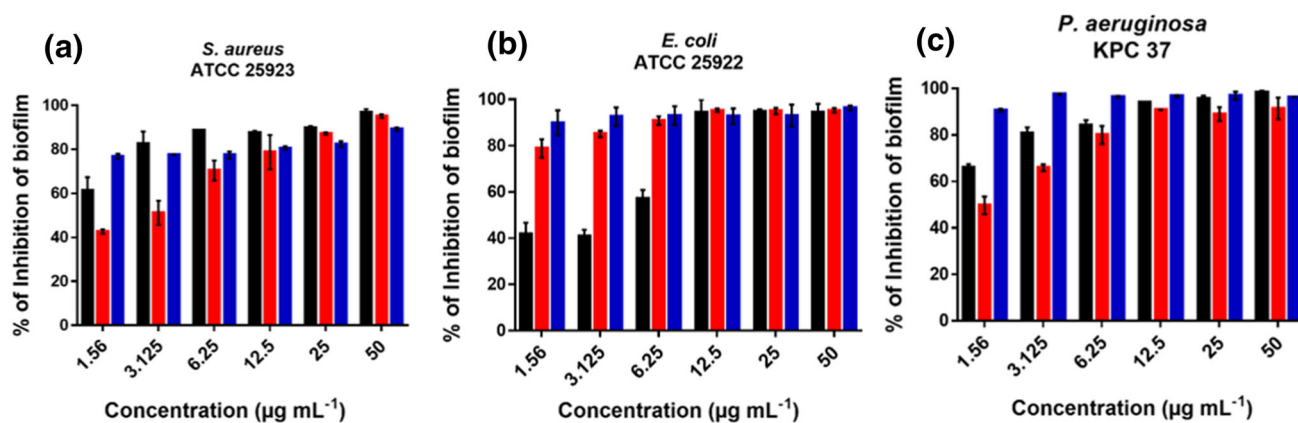


Fig. 9 Effect of biosynthesized AgNPs-GT (black bars), AgNPs-D (red bars) and AgNPs-F (blue bars) on *S. aureus* ATCC 25923 (a), *E. coli* ATCC 25922 (b) and *Pseudomonas aeruginosa* KPC 37 (c) biofilm formation

by antibiotic resistance and by evading host immune responses. Biofilms are highly impermeable leading to antibiotic resistant (Parrino et al. 2019). In the current study, the ability to inhibit biofilm formation of AgNPs-GT, AgNPs-D and AgNPs-F was evaluated against *S. aureus*, *E. coli* and the *P. aeruginosa* (Fig. 9a–c). Figure 9 shows the potent antibiofilm activity of all synthesized AgNPs against different bacteria strains, at different nanoparticle concentrations.

In the case of *S. aureus* (Fig. 9a), it is possible to observe that at nanoparticle concentration of 50 µg mL⁻¹, all tested AgNPs were able to inhibit ca. 90% of biofilm formation, and ca. 80% of biofilm inhibition was observed for nanoparticle concentration of 12.5 µg mL⁻¹, for all tested AgNPs. Even the lowest tested concentration (1.56 µg mL⁻¹) of AgNP-F inhibited ca. 80% of *S. aureus* biofilm (Fig. 9a). In the case of *E. coli* (Fig. 9b), all tested AgNPs at concentration of 12.5 µg mL⁻¹ inhibited ca. 95% of biofilm. Interestingly, at the lowest tested concentration (1.56 µg mL⁻¹), AgNPs-F inhibited 90% of *E. coli* biofilm. In the case of *P. aeruginosa* (Fig. 9c), all tested nanoparticles at concentration 12.5 µg mL⁻¹ showed potent antibiofilm activity (ca. 97% of biofilm inhibition). In addition, *P. aeruginosa* was found to be very sensitive to AgNPs, with a strong inhibitory effect (almost 91%) at nanoparticle concentration of 1.56 µg mL⁻¹. AgNPs-GT and AgNPs-D presented a biofilm inhibition of more than 90% at nanoparticle concentration of 25 µg mL⁻¹ (Fig. 9c). Thus, in this study, a clinical *P. aeruginosa* strain, which is resistant to a variety of antibiotics, and has a strong capacity to form biofilms, was very susceptible to biogenically synthesized AgNPs-F.

Our results are in accordance with the previous published papers (Lotha et al. 2018). For instance, Kalishwaralal et al. synthesized AgNPs using a green route and demonstrated an antibiofilm activity against *P. aeruginosa*

and *S. epidermidis* biofilms with an inhibition of 95% to 98% at nanoparticle concentration of 100 nmol L⁻¹ of AgNPs (Kalishwaralal et al. 2010). In another work, Singh and collaborators (2018) produced AgNPs by using *Cannabis sativa* and demonstrated a potent antibiofilm efficacy of almost 100% against *P. aeruginosa*, *E. coli* and *S. epidermidis* (Singh et al. 2018). Studies report that bacteria within biofilms are more resistant to antibiotics than planktonic bacteria, making difficult to control the infections (Velázquez-velázquez et al. 2015). Our results demonstrated that AgNPs synthesized by green routes might be effectively used against biofilm formation, at low nanoparticle concentration.

3.7 Imaging of MDR *P. aeruginosa* KPC 37 biofilm using scanning confocal laser microscopy

Biofilms represent one of the major issues in bacterial infection, being ten thousand times more resistant in comparison with planktonic bacteria (Sonesson et al. 2017). In vitro tests indicated that biofilms were able to survive to common antibiotics treatment even at a concentration one thousand times higher than the necessary to inhibit free-floating bacteria (Stewart and Costerton 2001). *P. aeruginosa* biofilms commonly occur in various hospital settings, mostly in medical devices, such as catheters and ventilators and chronic lung infections (Taylor et al. 2014). Despite causing severe and chronic infections, *P. aeruginosa* biofilm rapidly develops antibiotic resistance leading to difficulty in antibiotic-based treatments (Folkesson et al. 2012; Jeukens et al. 2014). In contrast, AgNPs present a promising alternative in the combat of *P. aeruginosa* biofilms.

To quantify the percentage of live bacteria in the biofilm formed, live–dead staining was carried for MDR *P. aeruginosa* KPC 37 strain. The formation of *P. aeruginosa*

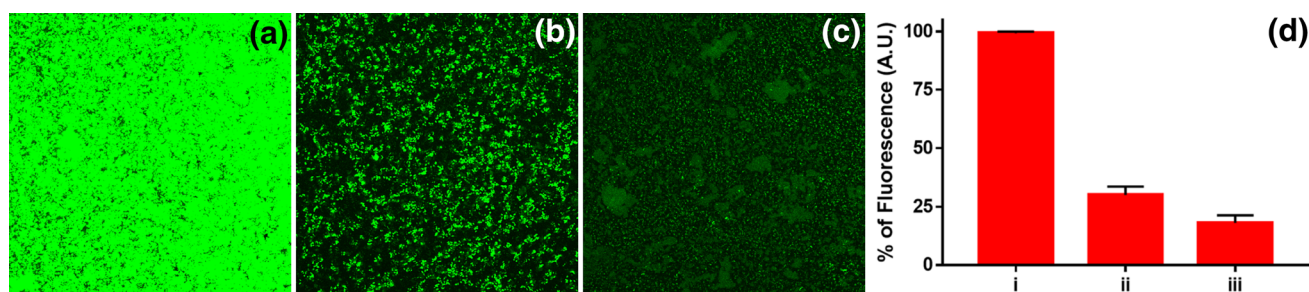


Fig. 10 Confocal micrograph images of MDR *Pseudomonas aeruginosa* KPC 37 biofilms. **a** Positive control (untreated biofilm); **b** biofilm incubated with AgNPs-GT at 50 µg mL⁻¹ and **c** biofilm incubated with AgNPs-GT at 100 µg mL⁻¹. Green cells are viable.

d Efficacy of MDR *P. aeruginosa* KPC 37 biofilm destruction, upon incubation with AgNPs-GT at (ii) 50 µg mL⁻¹ and (iii) 100 µg mL⁻¹. (i) Negative control

KPC 37 biofilm was carried out on the sample holder for confocal microscopy. After 24 h of incubation, the medium was removed and a fresh medium containing AgNPs-GT, at concentrations of 50 or 100 µg mL⁻¹, was added. The biofilm viability was analyzed using confocal laser scanning microscopy. This technique allows the evaluation of the efficacy of nanoparticles in the elimination of formed *P. aeruginosa* KPC 37 biofilm. Results are shown in Fig. 10. Figure 10a shows the confocal microscope image of *P. aeruginosa* KPC 37 biofilm without treatment (control group). Figure 10b, c shows the images of viable biofilm after the biofilm treatment with AgNPs-GT (50 or 100 µg mL⁻¹, respectively). In this work, AgNPs-GT was selected to demonstrate the efficacy of biogenic synthesized nanoparticles against biofilm, since AgNPs-GT showed lower MBC value, compared with AgNPs-F, and superior phenolic content and antioxidant activity compared with AgNPs-D. Moreover, the previous results from our group demonstrated potent antibacterial activity of AgNPs-GT (Rolim et al. 2019a, Rolim et al. 2019b). Live bacteria appeared green in the images after the treatment. Fluorescence intensity of positive control (control—Fig. 10a) was taken as 100%, and fluorescence of other images was quantified relative to the control. Figure 10d shows the fluorescence intensities of the biofilms. It is possible to observe higher fluorescence intensity for the lowest tested nanoparticle concentration (50 µg mL⁻¹). The treatment of *P. aeruginosa* KPC37 biofilm with 100 µg mL⁻¹ of AgNPs-GT caused bacteria death of more than 75%.

By comparing results in Fig. 9 with Fig. 10d, it is possible to observe that nanoparticle concentrations that are able to avoid almost 100% of biofilm formation (Fig. 9) were not sufficient to kill biofilm cells after the establishment of the biofilm (Fig. 10d). Radzig and coauthors (2013) observed the same behavior for AgNPs against biofilms of *E. coli* AB1157 (Radzig et al. 2013). In other work, Oliver and coauthors observed that catechin, the major constituent of green tea, can exert antibiofilm

activity of *P. aeruginosa* by attenuation of quorum sensing (Oliver et al. 2018). Thus, Fig. 10d shows that AgNPs-GT is effective in killing bacteria in established MDR *P. aeruginosa* KPC 37 biofilms. Our results are in accordance with the previous papers (Lotha et al. 2018). It should be noted that biofilms of *P. aeruginosa* KPC 37 are very resistant. Even though, green synthesized AgNPs were able to kill bacteria in established and resistant biofilms. This result suggests the potent applications of green synthesized AgNPs in the combat of resistant bacterial infections.

4 Conclusions

This study describes the green synthesis of AgNPs by using plant extracts of green tea and dill and by using the mycelium-free extract produced by the white-root *S. hirsutum*, a white-root Chilean fungus. All plant extracts used in the green synthesis of AgNPs demonstrated a high phenolic content and thus a potent antioxidant activity. Several physicochemical and morphological characterizations of synthesized AgNPs were performed demonstrating the formation of small spherical particles at the nanoscale, coated with plant or fungus extracts. The prepared nanoparticles showed potent antioxidant and antibacterial activity, with relative low values of MIC and MBC (in the range of 1.56–25 µg mL⁻¹) against Gram-positive and Gram-negative bacteria. Overall, AgNPs-D showed lower values of MIC and MBC, compared to other nanoparticles. Furthermore, the synthesized AgNPs demonstrated a potent antibiofilm activity, at low nanoparticle concentration. AgNPs-F demonstrated higher percentage of biofilm inhibition, in comparison with the other nanoparticles, at the lowest tested nanoparticle concentration (1.56 µg mL⁻¹), against all tested bacterial strains. AgNPs-GT was efficiently applied in the disruption of MDR *P. aeruginosa* KPC37 biofilms. Thus, all synthesized nanoparticles reported here might find important biomedical applications,

especially in the treatment of multiresistant bacteria in clinical settings.

Acknowledgements We have appreciated the support from CNPq (404815/2018-9), FAPESP- CONICYTE (2018/08194-2, 2018/02832-7), CONICYT/FONDAP/15130015 and CONICYTE-REDES 180003. This study was financed in part by the Coordenação de Aperfeiçoamento de Pessoal de Nível Superior—Brasil (CAPES)—Finance Code 001.

Compliance with ethical standards

Conflict of interest On behalf of all authors, the corresponding author states that there is no conflict of interest.

References

- Ali SG, Ansari MA, Khan HM, Jalal M, Mahdi AA, Cameotra SS (2018) Antibacterial and antibiofilm potential of green synthesized silver nanoparticles against Imipenem resistant clinical isolates of *Pseudomonas aeruginosa*. *Bionanoscience* 8:544–553. <https://doi.org/10.1007/s12668-018-0505-8>
- Alsammarrarie FK, Wang W, Zhou P, Mustapha A, Lin M (2018) Green synthesis of silver nanoparticles using turmeric extracts and investigation of their antibacterial activities. *Colloids Surf B Biointerfaces* 171:398–405. <https://doi.org/10.1016/j.colsurfb.2018.07.059>
- Ansari Z, Saha A, Singha SS, Sen K (2018) Phytomediated generation of Ag, CuO and Ag-Cu nanoparticles for dimethoate sensing. *J Photochem Photobiol A Chem* 367:200–211. <https://doi.org/10.1016/j.jphotochem.2018.08.026>
- Asghar MA, Zahir E, Shahid SM, Khan MN, Asghar MA, Iqbal J, Walker G (2018) Iron, copper and silver nanoparticles: green synthesis using green and black tea leaves extracts and evaluation of antibacterial, antifungal and aflatoxin B1 adsorption activity. *LWT-Food Sci Technol* 90:98–107. <https://doi.org/10.1016/j.lwt.2017.12.009>
- Baber R, Mazzei L, Thanh NTK, Gavriilidis A (2017) An engineering approach to synthesis of gold and silver nanoparticles by controlling hydrodynamics and mixing based on a coaxial flow reactor. *Nanoscale* 9:14149–14161. <https://doi.org/10.1039/c7nr04962e>
- Basavaraja S, Balaji SD, Lagashetty A, Rajasab AH (2008) Extracellular biosynthesis of silver nanoparticles using the fungus *Fusarium semitectum*. *Mater Res Bull* 43:1164–1170. <https://doi.org/10.1016/j.materresbull.2007.06.020>
- Cuevas R, Durán N, Diez MC, Tortella GR, Rubilar O (2015) Extracellular biosynthesis of copper and copper oxide nanoparticles by *Stereum hirsutum*, a native white-rot fungus from Chilean forests. *J Nanomater* 10:1–7. <https://doi.org/10.1155/2015/789089>
- de Lima R, Seabra AB, Durán N (2012) Silver nanoparticles : a brief review of cytotoxicity and genotoxicity of chemically and biogenically synthesized nanoparticles. *J Appl Toxicol* 32:867–879. <https://doi.org/10.1002/jat.2780>
- de Oliveira Silva BS, Seabra AB (2016) Characterization of iron nanoparticles produced with green tea extract: a promising material for nitric oxide delivery. *Biointerface Res Appl Chem* 6:1280–1287
- Dubey SP, Lahtinen M, Sillanpää M (2010) Green synthesis and characterizations of silver and gold nanoparticles using leaf extract of *Rosa rugosa*. *Colloids Surf A Physicochem Eng Asp* 364:34–41. <https://doi.org/10.1016/j.colsurfa.2010.04.023>
- Duran N, Seabra AB (2018) Biogenic synthesized Ag/Au nanoparticles: production, characterization, and applications. *Curr Nanosci* 14:82–94. <https://doi.org/10.2174/1573413714666171207160637>
- Durán N, Marcato PD, Alves OL, De Souza GIH, Esposito E (2005) Mechanistic aspects of biosynthesis of silver nanoparticles by several *Fusarium oxysporum* strains. *J Nanobiotechnol* 3:1–7. <https://doi.org/10.1186/1477-3155-3-8>
- Durán N, Durán M, de Jesus MB, Seabra AB, Fávoro WJ, Nakazato G (2016a) Silver nanoparticles: a new view on mechanistic aspects on antimicrobial activity. *Nanomedicine* 12:789–799. <https://doi.org/10.1016/j.nano.2015.11.016>
- Durán N, Nakazato G, Seabra AB (2016b) Antimicrobial activity of biogenic silver nanoparticles, and silver chloride nanoparticles: an overview and comments. *Appl Microbiol Biotechnol* 100:6555–6570. <https://doi.org/10.1007/s00253-016-7657-7>
- Ebrahiminezhad A, Zare-Hoseinabadi A, Sarmah AK, Taghizadeh S, Ghasemi Y, Berenjian A (2018) Plant-mediated synthesis and applications of iron nanoparticles. *Mol Biotechnol* 60:154–168. <https://doi.org/10.1007/s12033-017-0053-4>
- Fahimirad S, Ajallouei F, Ghorbanpour M (2019) Synthesis and therapeutic potential of silver nanomaterials derived from plant extracts. *Ecotoxicol Environ Saf* 168:260–278. <https://doi.org/10.1016/j.ecoenv.2018.10.017>
- Fernández JG, Fernández-Baldo MA, Berni E, Camí G, Durán N, Raba J, Sanz MI (2016) Production of silver nanoparticles using yeasts and evaluation of their antifungal activity against phytopathogenic fungi. *Process Biochem* 51:1306–1313. <https://doi.org/10.1016/j.procbio.2016.05.021>
- Fierascu RC, Ion RM, Dumitriu I (2010) Noble metals nanoparticles synthesis in plant extracts. *Optoelectron Adv Mater Rapid Commun* 4:1297–1300
- Flores-López LZ, Espinoza-Gómez H, Somanathan R (2019) Silver nanoparticles: electron transfer, reactive oxygen species, oxidative stress, beneficial and toxicological effects Mini review. *J Appl Toxicol* 39:16–26. <https://doi.org/10.1002/jat.3654>
- Folkesson A, Jelsbak L, Yang L, Johansen HK, Ciofu O, Hoiby N, Molin S (2012) Adaptation of *Pseudomonas aeruginosa* to the cystic fibrosis airway: an evolutionary perspective. *Nat Rev Microbiol* 10:841–851. <https://doi.org/10.1038/nrmicro2907>
- Furusawa C, Horinouchi T, Maeda T (2018) Toward prediction and control of antibiotic-resistance evolution. *Curr Opin Biotechnol* 54:45–49. <https://doi.org/10.1016/j.copbio.2018.01.026>
- Garg S, Garg A (2018) Encapsulation of curcumin in silver nanoparticle for enhancement of anticancer drug delivery. *Int J Pharm Sci Res* 9:1160–1166. [https://doi.org/10.13040/IJPSR.0975-8232.9\(3\).1160-66](https://doi.org/10.13040/IJPSR.0975-8232.9(3).1160-66)
- Guo C, Zhou L, Lv J (2013) Effects of expandable graphite and modified ammonium polyphosphate on the flame-retardant and mechanical properties of wood flour-polypropylene composites. *Polym Polym Compos* 21:449–456. <https://doi.org/10.1002/app>
- Gurunathan S, Han JW, Kwon DN, Kim JH (2014) Enhanced antibacterial and anti-biofilm activities of silver nanoparticles against gram-negative and gram-positive bacteria. *Nanoscale Res Lett* 9:1–17. <https://doi.org/10.1186/1556-276X-9-373>
- Han L, Wang P, Zhu C, Zhai Y, Dong S (2011) Facile solvothermal synthesis of cube-like Ag@AgCl: a highly efficient visible light photocatalyst. *Nanoscale* 3:2931–2935. <https://doi.org/10.1039/c1nr10247h>
- Ignat I, Volf I, Popa VI (2011) A critical review of methods for characterisation of polyphenolic compounds in fruits and vegetables. *Food Chem* 126:1821–1835. <https://doi.org/10.1016/j.foodchem.2010.12.026>
- Jeukens J, Boyle B, Kukavica-Ibrulj I, Ouellet MM, Aaron SD, Charette SJ, Fothergill JL, Tucker NP, Winstanley C, Levesque RC (2014) Comparative genomics of isolates of a *Pseudomonas aeruginosa* epidemic strain associated with chronic lung

- infections of cystic fibrosis patients. *PLoS ONE* 9:1–15. <https://doi.org/10.1371/journal.pone.0087611>
- Kalangi SK, Dayakar A, Gangappa D, Sathyavathi R, Maurya RS, Narayana Rao D (2016) Biocompatible silver nanoparticles reduced from *Anethum graveolens* leaf extract augments the antileishmanial efficacy of miltefosine. *Exp Parasitol* 170:184–192. <https://doi.org/10.1016/j.exppara.2016.09.002>
- Kalishwaralal K, Barathmanikant S, Ram S, Pandian K, Deepak V, Gurnathan S (2010) Silver nanoparticles impede the biofilm formation by *Pseudomonas aeruginosa* and *Staphylococcus epidermidis*. *Colloids Surf B Biointerfaces* 79:340–344. <https://doi.org/10.1016/j.colsurfb.2010.04.014>
- Krishna G, Kumar SS, Pranitha V, Alha M, Charaya S (2015) Biogenic synthesis of silver nanoparticles and their synergistic effect with antibiotics: a study against *Salmonella* sp. *Int J Pharm Pharm Sci* 7:84–88
- Kumar A, Singh M, Singh PP, Singh SK, Raj P, Pandey KD (2016) Antioxidant efficacy and curcumin content of turmeric (*Curcuma longa* L.) flower. *Int J Curr Pharm Rev Res* 8:112–114
- Lotha R, Shamprasad BR, Sundaramoorthy NS, Ganapathy R, Nagarajan S, Sivasubramanian A (2018) Zero valent silver nanoparticles capped with capsaicinoids containing *Capsicum annum* extract, exert potent anti-biofilm effect on food borne pathogen *Staphylococcus aureus* and curtail planktonic growth on a zebrafish infection model. *Microb Pathog* 124:291–300. <https://doi.org/10.1016/j.micpath.2018.08.053>
- Machado S, Pinto SL, Grosso JP, Nows HPA, Albergaria JT (2013) Green production of zero-valent iron nanoparticles using tree leaf extracts. *Sci Total Environ* 445–446:1–8. <https://doi.org/10.1016/j.scitotenv.2012.12.033>
- Masek A, Chrzescijanska E, Latos M, Zaborski M, Podsedek A (2017) Antioxidant and antiradical properties of green tea extract compounds. *Int J Electrochem Sci* 12:6600–6610. <https://doi.org/10.20964/2017.07.06>
- Mehta SK, Chaudhary S, Gradzielski M (2010) Time dependence of nucleation and growth of silver nanoparticles generated by sugar reduction in micellar media. *J Colloid Interface Sci* 343:447–453. <https://doi.org/10.1016/j.jcis.2009.11.053>
- Mittal AK, Kaler A, Banerjee UC (2012) Free radical scavenging and antioxidant activity of silver nanoparticles synthesized from flower extract of *Rhododendron dauricum*. *Nano Biomed Eng* 4:118–124. <https://doi.org/10.5101/nbe.v4i3.p118-124.1>
- Mittal AK, Kumar S, Banerjee UC (2014) Quercetin and gallic acid mediated synthesis of bimetallic (silver and selenium) nanoparticles and their antitumor and antimicrobial potential. *J Colloid Interface Sci* 431:194–199. <https://doi.org/10.1016/j.jcis.2014.06.030>
- Mühling M, Bradford A, Readman JW, Somerfield PJ, Handy RD (2009) An investigation into the effects of silver nanoparticles on antibiotic resistance of naturally occurring bacteria in an estuarine sediment. *Mar Environ Res* 68:278–283. <https://doi.org/10.1016/j.marenvres.2009.07.001>
- Naika HR, Lingaraju K, Manjunath K, Kumar D, Nagaraju G, Suresh D, Nagabhushana H (2015) Green synthesis of CuO nanoparticles using *Gloriosa superba* L. extract and their antibacterial activity. *J Taibah Univ Sci* 9:7–12. <https://doi.org/10.1016/j.jtusci.2014.04.006>
- Nakurte I, Stankus K, Virsis I, Paze A, Rizhikovs J (2017) Characterization of antioxidant activity and total phenolic compound content of birch outer bark extracts using micro plate assay. *Environ Technol Resour Proc Int Sci Pract Conf* 1:197–201. <https://doi.org/10.17770/etr2017vol1.2554>
- Neethu S, Midhun SJ, Radhakrishnan EK, Jyothis M (2018) Green synthesized silver nanoparticles by marine endophytic fungus *Penicillium polonicum* and its antibacterial efficacy against biofilm forming, multidrug-resistant *Acinetobacter baumannii*. *Microb Pathog* 116:263–272. <https://doi.org/10.1016/j.micpath.2018.01.033>
- Niraimathi KL, Sudha V, Lavanya R, Brindha P (2013) Biosynthesis of silver nanoparticles using *Alternanthera sessilis* (Linn.) extract and their antimicrobial, antioxidant activities. *Colloids Surf B Biointerfaces* 102:288–291. <https://doi.org/10.1016/j.colsurfb.2012.08.041>
- Oliver S, Wagh H, Liang Y, Yang S, Boyer C (2018) Enhancing the antimicrobial and antibiofilm effectiveness of silver nanoparticles prepared by green synthesis. *J Mater Chem B* 6:4124–4138. <https://doi.org/10.1039/c8tb00907d>
- Oves M, Khan MS, Zaidi A, Ahmed AS, Ahmed F, Ahmad E, Sherwani A, Owais M, Azam A (2013) Antibacterial and cytotoxic efficacy of extracellular silver nanoparticles biofabricated from chromium reducing novel OS4 strain of *Stenotrophomonas maltophilia*. *PLoS ONE* 8:e59140. <https://doi.org/10.1371/journal.pone.0059140>
- Pal S, Ghosh D, Saha C, Chakrabarti AK, Datta SC, Dey SK (2012) Total polyphenol content, antioxidant activity and lipid peroxidation inhibition efficacy of branded tea (*Camellia sinensis*) available in India. *IJTS* 8:13–20
- Parrino B, Schillaci D, Carnevale I, Giovannetti E, Diana P, Cirrincione G, Cascioferro S (2019) Synthetic small molecules as anti-biofilm agents in the struggle against antibiotic resistance. *Eur J Med Chem* 161:154–178. <https://doi.org/10.1016/j.ejmech.2018.10.036>
- Radzigi MA, Nadochenko VA, Koksharova OA, Kiwi J, Lipasova VA, Khmel IA (2013) Antibacterial effects of silver nanoparticles on gram-negative bacteria: influence on the growth and biofilms formation, mechanisms of action. *Colloids Surf B Biointerfaces* 102:300–306. <https://doi.org/10.1016/j.colsurfb.2012.07.039>
- Rajasekharreddy P, Rani PU (2014) Biofabrication of Ag nanoparticles using *Sterculia foetida* L. seed extract and their toxic potential against mosquito vectors and HeLa cancer cells. *Mater Sci Eng, C* 39:203–212. <https://doi.org/10.1016/j.msec.2014.03.003>
- Ramadan M, Abd-Algader N, El-kamali H, Farrag AH, Ghanem K (2013) Volatile compounds and antioxidant activity of the aromatic herb *Anethum graveolens*. *J Arab Soc Med Res* 8:79–88. <https://doi.org/10.4103/1687-4293.123791>
- Ramírez-Aristizabal LS, Ortiz A, Ospina-Ocampo LF (2015) Evaluation of the antioxidant capacity and characterization of phenolic compounds obtained from tea (*Camellia Sinensis*) for products of different brands sold in Colombia. *Pharmacol Online* 3:149–159
- Rolim WR, Pelegrino MT, de Araújo Lima B, Ferraz LS, Costa FN, Bernardes JS, Rodrigues T, Brocchi M, Seabra AB (2019a) Green tea extract mediated biogenic synthesis of silver nanoparticles: characterization, cytotoxicity evaluation and antibacterial activity. *Appl Surf Sci* 463:66–74. <https://doi.org/10.1016/j.apsusc.2018.08.203>
- Rolim WR, Pieretti JC, Renó DLS, Lima BA, Nascimento MHM, Ambrosio FN, Lombello CB, Brocchi M, de Souza ACS, Seabra AB (2019b) Antimicrobial activity and cytotoxicity to tumor cells of nitric oxide donor and silver nanoparticles containing PVA/PEG films for topical applications. *ACS Appl Mater Interfaces* 11:6589–6604. <https://doi.org/10.1021/acsami.8b19021>
- Saeb ATM, Alshammari AS, Al-brahim H, Al-rubeaan KA (2014) production of silver nanoparticles with strong and stable antimicrobial activity against highly pathogenic and multidrug resistant bacteria. *Sci World J* 2014:1–9. <https://doi.org/10.1155/2014/704708>
- San AMM, Thongpraditchoe S, Sithisarn P, Gritsanapan W (2013) Total phenolics and total flavonoids contents and hypnotic effect

- in mice of *Ziziphus mauritiana* Lam. seed extract. Evidence-Based Complement Altern Med 2013:1–4. <https://doi.org/10.1155/2013/835854>
- Sarsar V, Selwal MK, Selwal KK (2015) Biofabrication, characterization and antibacterial efficacy of extracellular silver nanoparticles using novel fungal strain of *Penicillium atramentosum* KM. J Saudi Chem Soc 19:682–688. <https://doi.org/10.1016/j.jscs.2014.07.001>
- Seabra AB, Manosalva N, De Araujo Lima B, Pelegrino MT, Brocchi M, Rubilar O, Durán N (2017) Antibacterial activity of nitric oxide releasing silver nanoparticles. J Phys: Conf Ser 838:012031. <https://doi.org/10.1088/1742-6596/838/1/012031>
- Singh M, Mallick AK, Banerjee M, Kumar R (2016) Loss of outer membrane integrity in gram-negative bacteria by silver nanoparticles loaded with *Camellia sinensis* leaf phytochemicals: plausible mechanism of bacterial cell disintegration. Bull Mater Sci 39:1871–1878. <https://doi.org/10.1007/s12034-016-1317-5>
- Singh P, Pandit S, Garnæs J, Tunjic S, Mokkaapati VRSS, Sultan A, Thygesen A, Mackevica A, Mateiu RV, Daugaard AE, Baun A, Mijakovic I (2018) Green synthesis of gold and silver nanoparticles from *Cannabis sativa* (Industrial hemp) and their capacity for biofilm inhibition. Int J Nanomed 13:3571–3591. <https://doi.org/10.2147/IJN.S157958>
- Smith AW (2005) Biofilms and antibiotic therapy: is there a role for combating bacterial resistance by the use of novel drug delivery systems? Adv Drug Deliv Rev 57:1539–1550. <https://doi.org/10.1016/j.addr.2005.04.007>
- Sonesson A, Przybyszewska K, Eriksson S, Mörgelin M, Kjellström S, Davies J, Potempa J, Schmidtchen A (2017) Identification of bacterial biofilm and the *Staphylococcus aureus* derived protease, staphopain, on the skin surface of patients with atopic dermatitis. Sci Rep 7:1–12. <https://doi.org/10.1038/s41598-017-08046-2>
- Stepanović S, Vuković D, Dakić I, Savić B, Švabić-Vlahović M (2000) A modified microtiter-plate test for quantification of staphylococcal biofilm formation. J Microbiol Methods 40:175–179. [https://doi.org/10.1016/S0167-7012\(00\)00122-6](https://doi.org/10.1016/S0167-7012(00)00122-6)
- Stewart PS, Costerton JW (2001) Antibiotic resistance of bacteria in biofilms. Lancet 358:135–138. <https://doi.org/10.4103/0974-8237.167866>
- Sudha A, Jeyakanthan J, Srinivasan P (2017) Green synthesis of silver nanoparticles using *Lippia nodiflora* aerial extract and evaluation of their antioxidant, antibacterial and cytotoxic effects. Resour Technol 3:506–515. <https://doi.org/10.1016/j.refit.2017.07.002>
- Taylor PK, Yeung ATY, Hancock REW (2014) Antibiotic resistance in *Pseudomonas aeruginosa* biofilms: towards the development of novel anti-biofilm therapies. J Biotechnol 191:121–130. <https://doi.org/10.1016/j.jbiotec.2014.09.003>
- Vázquez G, Fontenla E, Santos J, Freire MS, González-Álvarez J, Antorrena G (2008) Antioxidant activity and phenolic content of chestnut (*Castanea sativa*) shell and eucalyptus (*Eucalyptus globulus*) bark extracts. Ind Crops Prod 28:279–285. <https://doi.org/10.1016/j.indcrop.2008.03.003>
- Velázquez-velázquez JL, Santos-flores A, Araujo-meléndez J, Sánchez-sánchez R, Velasquillo C, González C, Martínez-castañón G, Martínez-gutierrez F (2015) Anti-biofilm and cytotoxicity activity of impregnated dressings with silver nanoparticles. Mater Sci Eng C 49:604–611. <https://doi.org/10.1016/j.msec.2014.12.084>
- Verma P, Maheshwari SK (2019) Applications of silver nanoparticles in diverse sectors. Int J Nano Dimens 10:18–36. <https://doi.org/10.22034/ijnd.2018.87646.1609>
- Zayed MF, Eisa WH, Shabaka AA (2012) Malva parviflora extract assisted green synthesis of silver nanoparticles. Spectrochim Acta Part A Mol Biomol Spectrosc 98:423–428. <https://doi.org/10.1016/j.saa.2012.08.072>
- Zhang P, Shao C, Zhang Z, Zhang M, Mu J, Guo Z, Liu Y (2011) In situ assembly of well-dispersed Ag nanoparticles (AgNPs) on electrospun carbon nanofibers (CNFs) for catalytic reduction of 4-nitrophenol. Nanoscale 3:3357–3363. <https://doi.org/10.1039/c1nr10405e>